AN ULTRASONIC METHOD FOR THE DETERMINATION OF THE J CONTOUR-INTEGRAL

Michael Janssen and Jan Zuidema*

A method is described for determining an applied stress tensor by means of ultrasonic shear waves. Results are presented showing the plane stress distribution in a large part of a loaded aluminium 2024-T351 compact tension specimen. Based upon this, numerical J-integration is performed along several contours. Comparison is made with a J-value estimated using LEFM.

INTRODUCTION

Mostly the evaluation of the fracture parameter J is based on energetic principles i.e. determination of load vs. load-displacement. However, multiple specimens are required with different crack lengths or in the case of some special geometries certain assumptions must be made regarding plastic material behaviour.

Many of these restrictions do not apply when using the original definition of J as a contour-integral. Consider an arbitrary shaped 2-dimensional body containing a crack as shown in figure (1). Nonlinear elastic material behaviour is assumed as an approximation for plastic behaviour under monotonic loading. Rice (1) defined:

$$J = \int_{\Gamma} (W n_1 - T_i \partial_1 u_i) ds \qquad (1)$$

where Γ = any contour surrounding crack tip
W = strain energy density
T_i = component traction vector on Γ

* Department of Materials Science, Delft University of Technology.

$\partial_j u_i = \frac{\partial u_i}{\partial x_j}$ with u_i = component displacement vector

n_i = component of outward directed unit vector normal to Γ

s = arc length Γ (positive when measured contraclockwise)

The path independent nature of J often permits Γ to be chosen outside a possible plastic zone at the crack tip. Material behaviour then is linear elastic along the whole of Γ, in which case the strain energy density, traction vector and displacement gradient can be expressed in terms of components of stress and rotation. In its turn the rotation can be calculated from stress gradients if a rotation value is known at one point at least.

This means it is possible to evaluate J if the stress components and the gradients of the stress components are known along a contour in linear elastic material. In the investigation reported here, this information is obtained by measuring the complete distribution of the stress tensor around a crack tip. A technique using ultrasonic shear waves is applied which is based on acoustoelasticity i.e. the effect of stress on the propagation of acoustic waves. Shear waves have the potential of determining all three plane stress components.

ACOUSTOELASTIC STRESS DETERMINATION

Theory

Reference (2) describes more fully the theory concerning stress tensor determination by means of ultrasonic shear waves. The method relates to 2-dimensional geometries i.e. plates or sheets which consist of elastic material exhibiting a slight orthotropy. This is a form of anisotropy generally found in rolled material and can be characterized by an orthogonal set of 2-fold symmetry axes, denoted as plate axes x_1, x_2, x_3. The assumption is made that one of these, the x_3-axis, is normal to the plate surface. Measurements are carried out with shear waves travelling in this direction. These waves will show birefringence, i.e. an incident shear wave with an arbitrary polarization (particle displacement direction) will be split up into two waves polarized in the x_1 and x_2-direction. Their velocities will generally differ slightly.

Applying a load in the x_1, x_2-plane results in small changes in plate thickness and wave velocities and also a rotation of the polarization can be observed. Figure 2 shows this stress induced rotation α which in fact is a rotation of the orthotropic symmetry axes x_1', x_2', x_3' of stressed material around the x_3 plate axis.

The applied stress tensor σ can be expressed in terms of a 4th order k-tensor and a 2nd order τ-tensor:

$$\sigma_{ij} = k_{ijkl}\,\tau_{kl} \qquad i,j = 1,2 \tag{2}$$

The τ-tensor contains the acoustic data of unstressed and stressed material. Denoting the time-of-flight of the shear wave polarized in x_i'-direction by t_i, the following definition is used:

$$\tau_{ij} = \frac{\Delta t_{ij}}{t} \qquad i,j = 1,2 \tag{3}$$

where Δ = change caused by applied stress

$t_{11} = t_1 \cos^2\alpha + t_2 \sin^2\alpha$

$t_{22} = t_1 \sin^2\alpha + t_2 \cos^2\alpha$

$t_{21} = t_{12} = \frac{1}{2}(t_1 - t_2)\sin 2\alpha$

t = average time-of-flight

The k-tensor describes the acoustoelastic behaviour of the material for either plane stress or plane strain situations. Uniaxial tensile tests were used to determine this tensor for the aluminium alloy 2024-T351. As expected, an orthotropic behaviour was found with symmetry axes coinciding with the plate axes. Applying Voigt notation, which is possible because of the symmetrical σ- and τ-tensor, the k-components for this case of plane stress are (GPa):

$$\begin{pmatrix} k_{11} & k_{12} & k_{16} \\ k_{21} & k_{22} & k_{26} \\ k_{61} & k_{62} & k_{66} \end{pmatrix} = \begin{pmatrix} 51{,}2 & 21{,}8 & 0 \\ 22{,}5 & 42{,}5 & 0 \\ 0 & 0 & 15{,}0 \end{pmatrix}$$

defined on the plate axes with x_1 normal to the rolling direction.

Experimental procedure

Measurements of time-of-flight and polarization angle are carried out by means of a pulse-echo method. A highly damped 20 MHz normal incidence shear wave transducer with a diameter of 6 mm acts as transmitter and receiver.

Coupling between transducer and specimen. A viscous fluid is used to provide the acoustical coupling with the specimen. Because the acoustoelastic effect is so small this coupling layer is a weak link in the measurement. Within this layer additional reflections cause distortions in the waveshape. In practice these are not reproducable because of variations in the thickness and acoustical properties of the coupling fluid. This problem was solved by using a thicker layer (approx. 80 µm). This delays the reflections, so that at least the first part of the echo's are free of distortion. A specially designed holder is used to position the transducer exactly parallel to the specimen surface and at the required distance.

Polarization angle measurement. The holder also allows rotation of the transducer i.e. variation of the polarization angle of the transmitter/receiver. In general the received signal will contain both birefringent waves in a certain ratio. Often they will overlap in time owing to the slight difference in velocity. However, there are always two transducer polarization angles normal to each other at which extinction of one of both waves takes place. This angle can be recognized by a maximum or minimum in the received signal amplitude during rotation. By coupling the transducer to a potentiometer the polarization angle can be measured with an accuracy of 1^{o}.

Time-of-flight measurement. With one of the birefringent waves extinguished the time-of-flight of the other can be measured. A counter/timer is used with a clock frequency of 100 MHz. Averaging over 1000 measurements provides a resolution of 1/3 ns. To avoid interference from the delayed reflections in the coupling layer, the first zero crossing in the echo is used for triggering.

J-EVALUATION FOR A COMPACT TENSION SPECIMEN

The stress tensor field around the crack tip

In order to evaluate the J-integral, the stress distribution in a large part of a compact tension specimen was determined by means of the technique described above. Figure 3 shows the aluminium 2024-T351 specimen, with the grid of 12 x 12 measuring points, 10 mm apart, arranged symmetrically around the crack tip.

Acoustic measurements were performed in the unloaded state and with a tensile load of 8200 N.

A problem encountered during this experiment was the influence of temperature on the time-of-flight. A temperature coefficient of $0{,}35 \cdot 10^{-3}\ K^{-1}$ was found. Since fluctuations in temperature during the lengthy experiment are inevitable, this effect can not be neglected. Therefore the specimen temperature was registered for each acoustical measurement and all times-of-flight were corrected afterwards.

Figure 4, 5 and 6 show the results in the form of lines of constant σ_{11}, σ_{22} and σ_{21} respectively. For the latter two stress components use was made of the fact that they are zero on the crack flanks. The patterns are symmetrical within approx. 10 MPa.

J-integrand in terms of stress

Applying the isotropic form of Hooke's law to the integrand of J (eq. 1) yields the following expression for the case of plane stress:

$$I_J = \frac{1}{E}\{\tfrac{1}{2}(\sigma_{22}{}^2 - \sigma_{11}{}^2)n_1 - \sigma_{21}(\sigma_{11} + \sigma_{22})n_2\} - \omega_{21}(\sigma_{21}n_1 + \sigma_{22}n_2) \tag{4}$$

where I_J = integrand J
E = Young's modulus
ω_{ij} = component rotation tensor = $\frac{1}{2}(\partial_j u_i - \partial_i u_j)$

A second application of Hooke's law enables the change of rotation between two neighbouring points to be written in terms of stress gradients. Again for plane stress:

$$d\omega_{21} = \frac{1}{E}[\{(1+\nu)\partial_1\sigma_{21} - \partial_2\sigma_{11} + \nu\partial_2\sigma_{22}\}dx_1 + -\{(1+\nu)\partial_2\sigma_{21} - \partial_1\sigma_{22} + \nu\partial_1\sigma_{11}\}dx_2] \tag{5}$$

where ν = Poisson's ratio
$\partial_k\sigma_{ij} = \frac{\partial\,\sigma_{ij}}{\partial\,x_k}$

Theoretically J only depends on the change in rotation along the contour Γ. A constant component of the rotation ω_{21} in eq. 4 will not contribute since $(\sigma_{21}n_1 + \sigma_{22}n_2)$ integrates to zero along Γ. However, experimental errors in σ_{22} and σ_{21} will cause a dependence of J on the absolute rotations. Therefore absolute values are estimated by assuming the rotation is zero on the mid-line of the specimen ahead of the crack tip, as the specimen is symmetrical.

Numerical J-integration

Integration is performed along five contours as shown in figure 7. Four of these (A, B, C and D) surround the crack tip at increasing distance. Contour E is closed and should thus give a zero J-value.

Rotations can be calculated at any point on a contour Γ by integrating $d\omega_{21}$ along many different paths starting from the mid-line. However, it is convenient if J-evaluation can be based on a smaller number of stress measurements compared to the 12 x 12 available. Therefore integration of equation 5 is done along Γ so the only data needed are those on and directly beside the contour. The resulting rotation values, adjusted so as to be zero ahead of the crack, are shown in figure 8. Symmetry is within 10% and furthermore integrating $d\omega_{21}$ round the closed contour E yields a value almost identical to the starting value.

The J-integrand values (fig. 9) show discontinuities. These are caused by the angular shape of the contours but have no consequences for the integration. Table 1 summarizes the results together with an estimate of J using linear elastic fracture mechanics, i.e.

based on the K_I-value for this specific geometry and load (ref. 3), corrected for the plastic zone size following Irwin (ref. 4). This should give a valid estimate since the plastic zone is much smaller than the specimen dimensions in the x_1, x_2-plane. Experimental values agree within 9% of this "theoretical" value. The closed contour J-value is small compared to the other values.

In table 1 the influence on J of a component of rotation that is constant along the whole contour ($dJ/d\omega$) is also indicated. As is argued above, experimental errors in σ_{22} and σ_{21} determine this quantity. For the worst case (contour B) it amounts to 0,9 N/mm per $\%_{oo}$.

TABLE 1 - Results of J-integration along several contours together with an estimate from LEFM.

	Contour A	B	C	D	Closed contour E	Estimate from LEFM
J(N/mm)	21,2	22,1	24,1	23,5	0,15	22,1
$dJ/d\omega$ (N/mm)	+290	-930	-480	-700	-380	-

CONCLUSION

An acoustoelastic determination of the distribution of normal stresses and shear stress around a crack in sheets of aluminium 2024-T351 appears to be feasable although a straightforward check using finite element calculations is still to be performed. Results of J-integration using discrete stress data agree within 9% of an estimate from LEFM. Furthermore, it is practicable only to use data on and directly beside a contour, i.e. a contour with finite width. The main reason for the spread in J-values and for the dependence on the absolute rotation values is probably the inaccuracy of the stress measurements. Improvement hereof is of prime importance.

Application of this technique to other more plastic materials and different geometries and loading conditions is promising.

SYMBOLS USED

E = Young's modulus (MPa)

I_J = integrand J (MPa)

J = fracture parameter (N/mm)

k_{ijkl} or k_{IJ} = component acoustoelastic tensor (GPa)

n_i = component outward directed unit vector normal to Γ (-)

s = arc-length Γ (mm)

T_i = component traction vector on Γ (MPa)

t = average time-of-flight (s)

t_i = time-of-flight shear wave polarized in x_i'-direction (s)

t_{ij} = alternatively defined time-of-flight (s)

u_i = component displacement vector (mm)

W = strain energy density (MJ/m^3)

x_i = orthogonal plate axes

x_i' = orthotropic symmetry axes

α = stress induced rotation of polarization (^{o})

Γ = J-contour

Δ = change caused by stress

∂_i = partial derivative with respect to x_i

ν = Poisson's ratio (-)

σ_{ij} = component stress tensor (MPa)

τ_{ij} = component tensor containing acoustic data (-)

ω_{ij} = component rotation tensor (-)

REFERENCES

(1) Rice, J.R., "Mathematical analysis in the mechanics of fracture" in "Fracture, an advanced Treatise", Ed. H. Liebowitz, Academic Press, New York, Vol. 2, pp. 192-311, 1968.

(2) Janssen, M. and Zuidema, J., J. of Nondestructive Evaluation, Vol. 5, No. 1, 1986.

(3) Tada, H., Paris, P.C. and Irwin, G.R., "The stress analysis of cracks Handbook", Del Research Corporation, Hellertown, Pennsylvania, 1973.

(4) Ewalds, H.L. and Wanhill, R.J.H., "Fracture Mechanics", D.U.M., Delft - Edward Arnold, London, 1984.

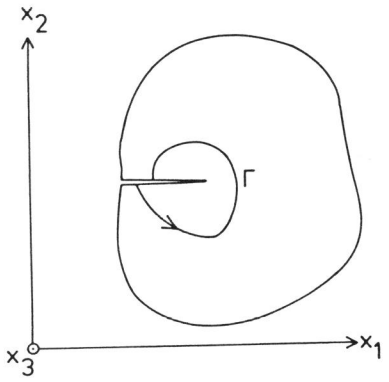

Figure 1. Two dimensional nonlinear elastic body.

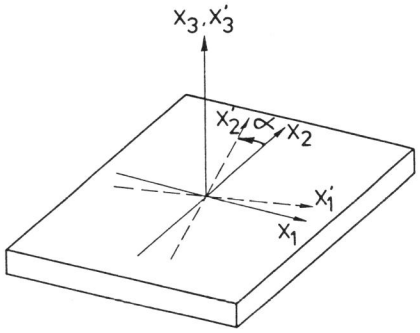

Figure 2. Stress induced rotation (α positive as drawn).

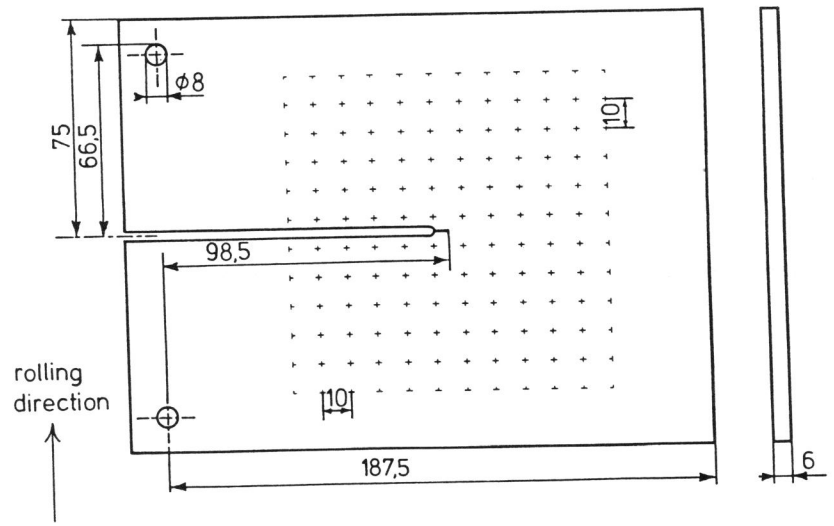

Figure 3. Geometry CT-specimen including grid of measuring points.

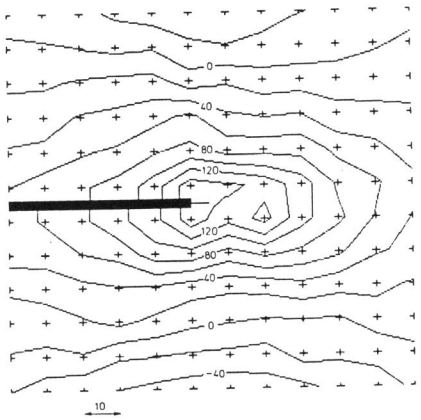

Figure 4. Measured distribution σ_{11}-component (MPa).

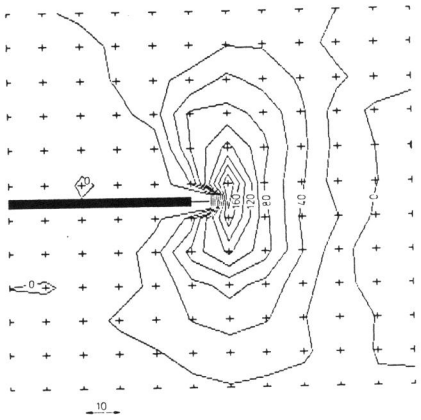

Figure 5. Measured distribution σ_{22}-component (MPa).

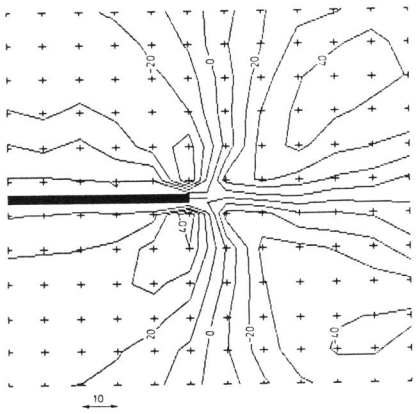

Figure 6. Measured distribution σ_{21}-component (MPa).

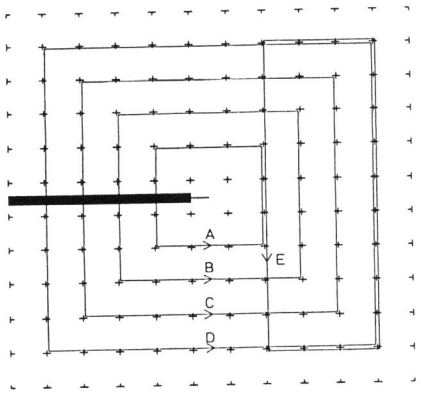

Figure 7. Contours considered for J-evaluation.

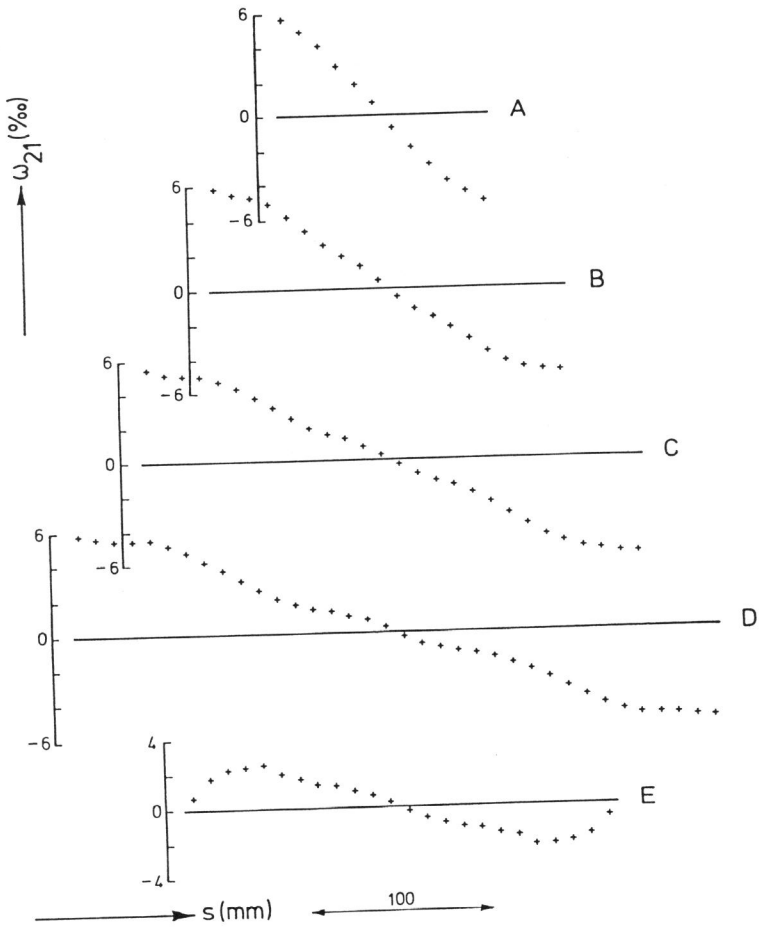

Figure 8. Calculated rotation ω_{21} as a function of arc-length s.

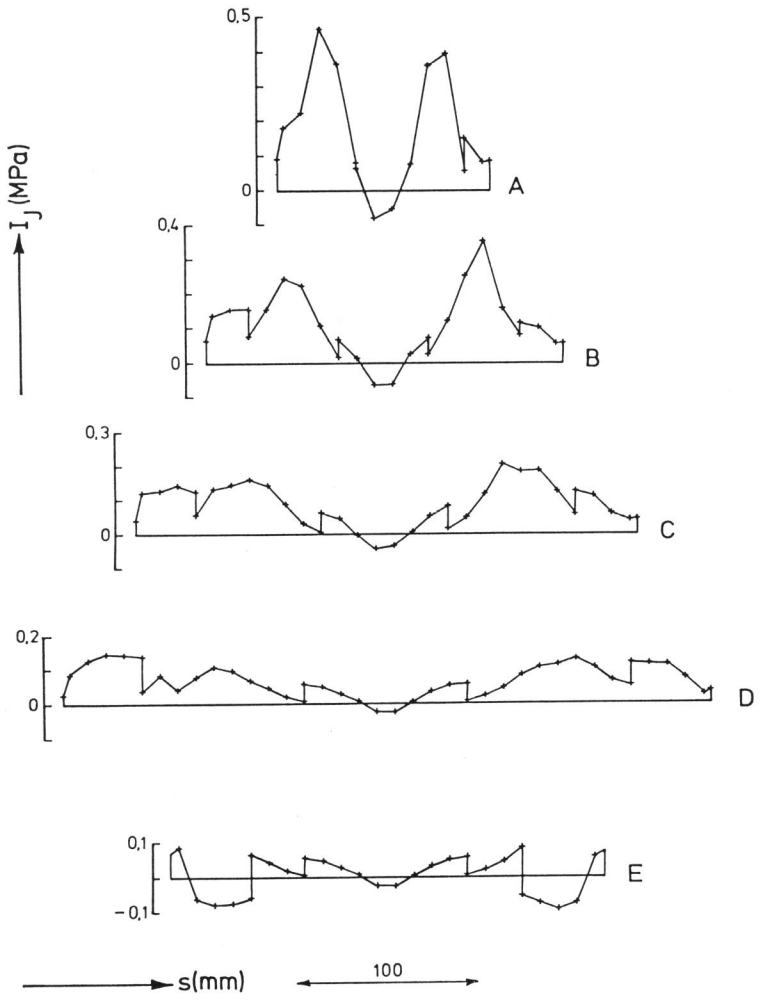

Figure 9. Calculated J-integrand I_J as a function of arc-length s.